

# Entanglement Properties of the One-Dimensional Dimerized Fermi-Hubbard Model

Min-Chul Cha<sup>1\*</sup>, Hoon Beom Kwon<sup>1</sup>, Ji-Woo Lee<sup>2</sup>, Myung-Hoon Chung<sup>3</sup>

<sup>1</sup> *Department of Photonics and Nanoelectronics, Hanyang University, Ansan 15588, Korea*

<sup>2</sup> *Department of Physics, Myongji University, Yongin 17058, Korea*

<sup>3</sup> *College of Science and Technology, Hongik University, Sejong 30016, Korea*

We study the entanglement properties of the one-dimensional dimerized Fermi-Hubbard model. Using a matrix-product-state approach, we compute the ground state and identify two insulating phases at 1/2- and 3/4-filling, along with a metallic phase, whose mechanisms can be characterized by their entanglement spectra. Our findings indicate that the two insulating phases are distinct, implying that the phase at 1/2-filling has a charge gap arising from the band gap, which is enhanced by repulsive interactions, while the phase at 3/4-filling exhibits a Mott gap resulting from particle interactions. This difference between the two insulating phases is reflected in the scaling properties of the half-chain entanglement entropy and the distribution of the entanglement spectrum.

## I. INTRODUCTION

Entanglement properties provide a powerful framework for exploring and understanding interacting quantum systems<sup>1-4</sup>. As one of the most distinctive features of quantum systems, entanglement marks quantum phase transitions and offers useful tools for analyzing the critical properties through the universal scaling behavior of entanglement entropy<sup>5-8</sup> and the universal distribution of the entanglement spectrum<sup>9-11</sup>. It is also useful for characterizing quantum phases, including topological properties<sup>12,13</sup>, which are often closely related to the energy gaps and the edge states that these gaps entail<sup>14-18</sup>. Significant efforts have been devoted to understanding how interactions modify these properties<sup>19-26</sup>.

The dimerized Fermi-Hubbard model, originally introduced to study the physical properties induced by dimerization in materials such as polyacetylene in the non-interacting limit<sup>27,28</sup>, serves as one of the simplest models for testing the usefulness of entanglement properties in characterizing quantum phases of interacting systems. This model is notable for exhibiting two different insulating phases arising from the interplay of interaction and dimerization, each with distinct properties, including topological aspects<sup>29,30</sup>. Entanglement properties can be a useful tool for revealing the differences between these two insulating phases. Many studies have focused on clarifying the bulk-edge correspondence between them through the entanglement entropy in this model<sup>31-35</sup>. Entanglement spectra have also been employed to study the topological properties<sup>36</sup>.

In this work, we study the dimerized Fermi-Hubbard model in one dimension, employing a matrix-product-state approach<sup>37-39</sup> to calculate the ground state. The ground state exhibits the two distinct insulating phases, at 1/2-filling and at 3/4 (or 1/4)-filling. At 1/2-filling, the charge gap arises from the band gap in the weak interaction region, which is further enhanced by repulsive on-site

interactions. (In the strong interaction limit, a Mott gap opens with the presence of antiferromagnetic ordering. Here, we focus on the case of moderately weak interactions.) On the other hand, at 3/4-filling, the Mott gap primarily results from interactions among particles. The differences between these two insulating phases elucidate the underlying physics of strongly correlated systems.

To investigate the differences, we analyze the entanglement properties of the system. The entanglement entropy serves as an important marker for differentiating the various phases of the model and enables us to construct the phase diagram. Our findings suggest that arbitrarily small repulsive interactions can open a charge gap in the 3/4-filled insulating phase. The scaling behavior of the entanglement entropy distinctly clarifies the different nature of these two insulating phases. Entanglement entropy also serves as an indicator of the edge states. In addition, each phase, including the metallic phase, can be identified by its characteristic structure appearing in the entanglement spectrum. The universal distribution of the entanglement spectrum further highlights the different nature of the two insulating phases.

## II. ONE-DIMENSIONAL DIMERIZED FERMION-HUBBARD MODEL

### A. $U = 0$

Let us consider the Hamiltonian of the one-dimensional dimerized Fermi-Hubbard model with staggered hopping amplitudes  $t_+ = t_0 + \delta t$  and  $t_- = t_0 - \delta t$ , given by

$$H = - \sum_{ij,\sigma} \mathbf{c}_{i\sigma}^\dagger \cdot \mathbf{T}_{ij} \cdot \mathbf{c}_{j\sigma} + U \sum_i (n_{iA,\uparrow} n_{iA,\downarrow} + n_{iB,\uparrow} n_{iB,\downarrow}) \quad (1)$$

with

$$\mathbf{T}_{ij} = \begin{pmatrix} (\mu + \frac{U}{2})\delta_{ij} & t_+\delta_{ij} + t_-\delta_{i,j+1} \\ t_+\delta_{ij} + t_-\delta_{i,j-1} & (\mu + \frac{U}{2})\delta_{ij} \end{pmatrix} \quad (2)$$

\*corresponding author: mccha@hanyang.ac.kr

and

$$\mathbf{c}_{j\sigma} = \begin{pmatrix} c_{jA,\sigma} \\ c_{jB,\sigma} \end{pmatrix}, \quad (3)$$

where we take two adjacent sites (sites  $A$  and  $B$ , belonging to  $A$ - and  $B$ -sublattices, respectively) coupled via  $t_+$  as a unit cell. Here,  $i$  and  $j$  are indices for the unit cells. The operators  $c_{jA,\sigma}$  ( $c_{jB,\sigma}$ ) and  $c_{jA,\sigma}^\dagger$  ( $c_{jB,\sigma}^\dagger$ ) represent the particle annihilation and creation operators, respectively, and  $n_{jA,\sigma}$  ( $n_{jB,\sigma}$ ) denote the particle number operators at sites  $A$  and  $B$  in the  $j$ -th cell, with  $\sigma = \uparrow, \downarrow$  representing the spin index.  $U$  is the on-site repulsion strength, and  $\mu$  is the chemical potential. Therefore, we consider  $t_+$  as the intra-cell coupling, while  $t_-$  serves as the intercell coupling. For convenience, we set  $t_0 = 1$  in our study.

In the non-interaction case ( $U = 0$ ), which is referred to as the Su-Schrieffer-Heeger model, the Hamiltonian can be reduced using the Fourier transformation

$$\begin{aligned} \tilde{\mathbf{c}}_{k\sigma} &= \frac{1}{\sqrt{L/2}} \sum_j e^{ikR_j} \mathbf{c}_{j\sigma}, \\ \mathbf{c}_{j\sigma} &= \frac{1}{\sqrt{L/2}} \sum_k e^{-ikR_j} \tilde{\mathbf{c}}_{k\sigma}, \end{aligned} \quad (4)$$

resulting in the form

$$H_0 = - \sum_{k,\sigma} \tilde{\mathbf{c}}_{k\sigma}^\dagger \cdot \begin{pmatrix} 0 & \tau_k e^{i\theta_k} \\ \tau_k e^{-i\theta_k} & 0 \end{pmatrix} \cdot \tilde{\mathbf{c}}_{k\sigma}, \quad (5)$$

where

$$\tau_k = 2[\cos^2 k + |\delta t|^2 \sin^2 k]^{1/2}, \quad (6)$$

and  $\theta_k = \tan^{-1}[t_- \sin 2k / (t_+ + t_- \cos 2k)]$ . Here,  $L$  is the number of sites,  $R_j = 2j$  denotes the position of the  $j$ -th unit cell for  $j = 1, \dots, L/2$ , and  $k = 2\pi n/L$  for an integer  $n$  ( $-L/4 < n \leq L/4$ ) is the wave number.

With an even integer  $L$  for the periodic boundary condition, we have energy levels given by

$$\epsilon_\pm(k) = \pm \tau_k. \quad (7)$$

A finite  $\delta t$  thus yields a band gap  $\Delta\epsilon = 4|\delta t|$  at the Brillouine zone boundary ( $k = \pi/2$ ), resulting in a band insulator at 1/2-filling, which is a typical example of a topological insulator<sup>28</sup>. Even for  $U > 0$ , we still expect that this band insulating property remains at 1/2-filling, with an enhanced charge gap due to the repulsive interactions for sufficiently large  $|\delta t|$ .

### B. $U > 0$

The most significant change introduced by  $U > 0$  is the opening of the Mott gap at 3/4 (or 1/4)-filling when there is a finite  $|\delta t|$ . To investigate this insulating phase, we employ the matrix-product-state (MPS) representation to effectively handle the interactions. This method also

provides entanglement properties that are very useful for identifying the different phases.

A canonical form of the MPS wavefunction<sup>37,38</sup> for the ground state is constructed as follows:

$$|\Psi\rangle = \sum_{\{s_i\}} A^{[s_1]} \Lambda_1 B^{[s_2]} \Lambda_2 C^{[s_3]} \Lambda_1 D^{[s_4]} \Lambda_2 A^{[s_5]} \dots D^{[s_L]} \Lambda_2 \times |s_1, s_2, s_3, s_4, \dots, s_L\rangle, \quad (8)$$

where the matrices  $A$ 's,  $B$ 's,  $C$ 's, and  $D$ 's are the MPS matrices of size  $\chi \times \chi$ ,  $\Lambda_1$  and  $\Lambda_2$  are vectors of size  $\chi$ , and  $s_\ell$  are physical indices for the basis states ( $|s_\ell\rangle = |0\rangle, |\uparrow\rangle, |\downarrow\rangle, |\uparrow\downarrow\rangle$ ) at the  $\ell$ -th site. We take the limit  $L \rightarrow \infty$  for an infinite chain. To obtain the correct wavefunction, we need to repeatedly multiply matrices in the form  $A^{[s_a]} \Lambda_1 B^{[s_b]} \Lambda_2 C^{[s_c]} \Lambda_1 D^{[s_d]} \Lambda_2$  especially near or at 3/4-filling. This differs from the form  $A^{[s_a]} \Lambda B^{[s_b]} \Lambda$  used when  $\delta t = 0$ . If we attempt to use the form  $A^{[s_a]} \Lambda_1 B^{[s_b]} \Lambda_2 C^{[s_c]} \Lambda_3 D^{[s_d]} \Lambda_4$  with four different  $\Lambda$ 's, we consistently find that  $\Lambda_1 = \Lambda_3$  and  $\Lambda_2 = \Lambda_4$ .

The lowest energy state is then obtained by using the time-evolving block decimation (TEBD) algorithm<sup>37,38</sup>. By dividing the imaginary time into small intervals of size  $\Delta\tau$ , we apply the Suzuki-Trotter decomposition  $e^{-\tau H} = (e^{-\Delta\tau H})^N$  ( $\Delta\tau = \tau/N$ ) to implement the two-site TEBD<sup>11</sup>. The number of repetitions  $N$  is determined under the condition that the energy difference between subsequent states is less than  $10^{-12}$ . A smaller  $\Delta\tau$  reduces the decomposition errors but requires a longer time for the TEBD process. We choose  $\Delta\tau = 0.001$  in our calculations, which costs a long time to compute but is necessary to obtain the lowest energy state, especially near the phase transition.

The elements of the vector  $\Lambda$  represent the Schmidt coefficients, which are non-negative real numbers. The half-chain entanglement entropy,  $S_h$ , is then defined by

$$S_h = - \sum_{\alpha=1} \lambda_\alpha^2 \log_2 \lambda_\alpha^2, \quad (9)$$

where  $\lambda_\alpha$  is the  $\alpha$ -th element of the vector  $\Lambda$  which bipartites the one-dimensional system. We also construct the reduced density matrix for a single-site and a double-site, and diagonalize them to obtain the corresponding entanglement entropies.

### III. ENTANGLEMENT PROPERTIES

The ground state wave functions obtained through MPS calculations using matrices of size  $\chi = 40$  provide the entanglement entropy and density, from which we can construct a phase diagram. Figure 1 shows a schematic phase diagram of the model for  $\delta t = 0.5$ . In the metallic phase, the density varies continuously as a function of the chemical potential  $\mu$ . In contrast, in the insulating phase, the density remains constant even as  $\mu$  varies. In addition to the insulating phase at 1/2-filling, another insulating

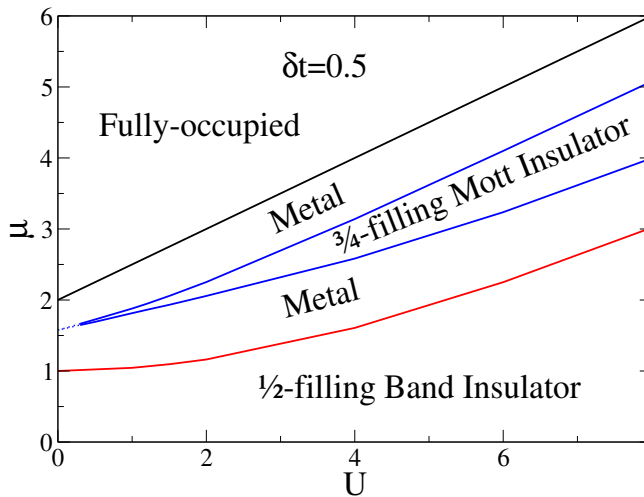


FIG. 1: Schematic phase diagram of the one-dimensional dimerized Fermi-Hubbard model for a dimerization strength of  $\delta t = 0.5$ . At 1/2-filling, a band insulating phase with band gap  $\Delta = 4\delta t$  emerges when  $U = 0$ , while at 3/4 (or 1/4)-filling a Mott insulating phase appears.

phase appears at 3/4 (or 1/4)-filling, which is characteristic of the dimerized Fermi-Hubbard model. Within our numerical accuracy, the gap opens for an arbitrarily small  $U$ . The charge gap at 1/2-filling is a band gap resulting from dimerization, in contrast to the ordinary Hubbard model<sup>40</sup> (i.e.,  $\delta t = 0$ ), where the charge gap is a Mott gap arising from interactions. On the other hand, at 3/4 filling, the Mott phase emerges due to interactions in the presence of dimerization.

Figure 2 shows the typical entanglement entropy for how much (a) a single-site, (b) a double-site, or (c) a half-chain region is correlated with the rest of the system when  $U = 2$  and  $\delta t = 0.5$ . The upper (black) lines represent the entanglement entropy when the region is coupled to the rest of the system via a  $t_+$ -bond, while the lower (red) lines correspond to the case of coupling via a  $t_-$ -bond. A single site always has one  $t_+$ -bond and one  $t_-$ -bond, ensuring that the black and red lines overlap. This behavior of entanglement entropy, along with the density behavior depicted in the inset, allows us to easily identify the occurrence of phase transitions. We can observe small peaks near the transition points, which are simply a consequence of the cluster mean-field behavior<sup>11</sup> that occurs in MPS numerical calculations using matrices of finite size.

Note that at 1/2-filling  $S_h \lesssim 2$  for the  $t_+$ -bond and  $S_h \gtrsim 0$  for the  $t_-$ -bond, which approach  $2 \log_2 2$  and 0, respectively, as  $U \rightarrow 0$  in the limit of  $|\delta t| \rightarrow 1$ . This has been considered as indicators of the edge states in the topologically non-trivial and topologically trivial states, respectively<sup>31</sup>. Our study shows that this behavior persists, albeit slightly modified by  $U > 0$ . Similarly,  $S_2$  approaches 4 and 2, respectively. This strongly suggests that the edge state properties representing the topologi-

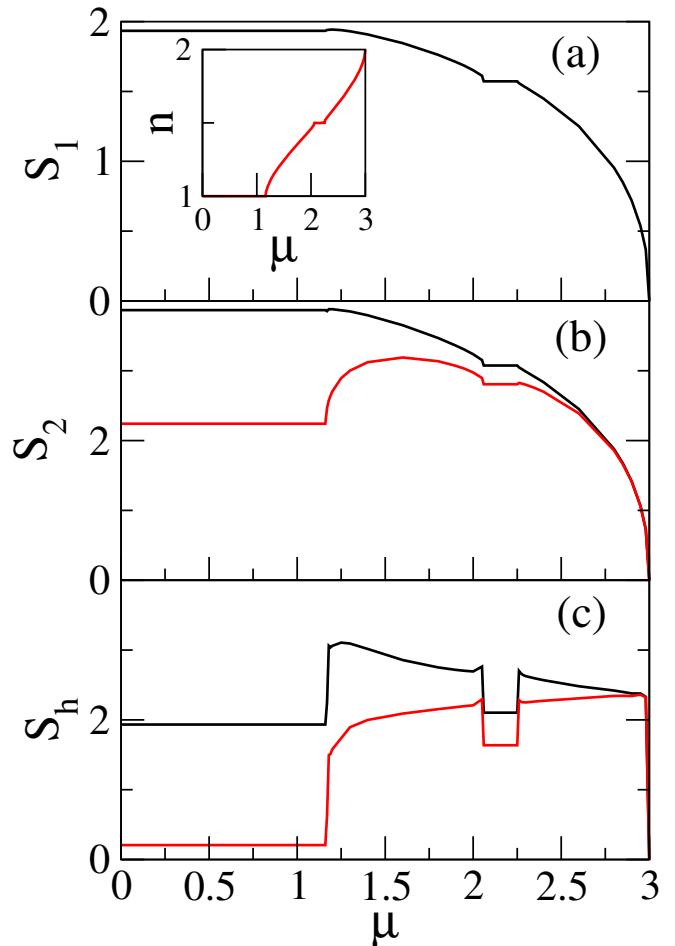


FIG. 2: Entanglement entropy for (a) a single-site (b) a double-site, and (c) a half-chain system as a function of  $\mu$  when  $U = 2$  and  $\delta t = 0.5$ . The black lines represent the entanglement entropy when the region is coupled to the rest of the system via a  $t_+$ -bond, while the lower red lines correspond to the case of coupling via a  $t_-$ -bond. In (a), the entanglement entropy shows overlapping black and red lines. The inset illustrates the density behavior, where the transitions between the insulating phase at fixed density and the metallic phase can be easily identified.

cal features still remain even for finite  $U$  and moderately large  $|\delta t|$ . However, these features are absent in the insulating phase at 3/4-filling, where the difference between  $S_h$  for the  $t_+$ -bond and the  $t_-$ -bond vanishes as  $U \rightarrow 0$ , even for a finite  $|\delta t|$ .

As mentioned above, we can identify two distinct insulating phases where the entanglement entropy and density remain unchanged as  $\mu$  varies. This implies that the wave functions are fixed in each insulating phase. It raises an intriguing question of whether these two insulating phases are fundamentally different. To clarify this, we investigate their entanglement properties. The behavior of a diverging correlation length  $\xi$  can be captured by the scaling relation  $S_h \sim (c/6) \log_2 \xi$  in one-dimensional systems, where  $c = 1$  is the central charge<sup>5,6</sup>. Furthermore,

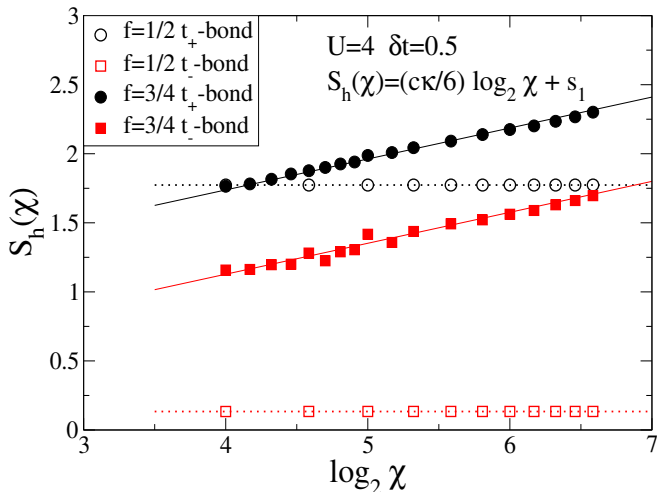


FIG. 3: Half-chain entanglement entropy  $S_h(\chi)$  in the insulating phases is plotted as a function of the matrix size  $\chi$  for  $U = 4$  and  $\delta t = 0.5$ . At 3/4-filling,  $S_h(\chi)$  exhibits a logarithmic scaling relation indicative of a Mott insulating phase, characterized by a correlation length with the exponent  $\kappa = 1.344$ . On the other hand, at 1/2-filling,  $S_h(\chi)$  shows minimal dependence on  $\chi$ , reflecting the properties of a gapped band insulator with finite correlation lengths. This difference shows the distinct nature of the two insulating phases.

$\xi$  can be characterized by  $\xi \sim \chi^\kappa$  with an exponent  $\kappa$  in an MPS with a finite matrix size  $\chi^{7,8}$ .

Figure 3 illustrates the half-chain entanglement entropy as a function of  $\chi$  in the insulating phases. The behavior at 3/4-filling follows the relation  $S_h(\chi) = (c\kappa/6)\log_2 \chi + s_1$  with  $\kappa = 1.344$  (where  $s_1$  represents some constants). This implies that it is a Mott insulating phase with a diverging correlation length, where the value of  $\kappa$  is consistent with theoretical predictions<sup>7</sup>, similar to the Mott phase of the ordinary half-filled Hubbard model<sup>39</sup>. However, at 1/2-filling,  $S_h(\chi)$  is found to be almost independent of  $\chi$ , indicating that in this insulating phase, correlation lengths are short and finite, which is a typical signature of a gapped band insulator. Thus, the scaling behavior of the half-chain entanglement entropy distinctly reveals a fundamental difference between the two insulating phases.

The entanglement properties of the phases are clearly revealed in the entanglement spectrum, which represents the distribution of the reduced density matrix eigenvalues. Figure 4 displays the typical half-chain entanglement spectrum in different phases for  $t_+$ - and  $t_-$ -bonds. Let us discuss the characteristics of the entanglement spectrum in each phase:

(1) We observe that the entanglement spectrum in the metallic phase exhibits double degeneracy for both  $t_+$ - and  $t_-$ -bonds, which is a hallmark of the metallic phase, as seen in the ordinary Hubbard model<sup>39</sup>. This double degeneracy is lifted in the insulating phases for  $t_-$ -bonds, as also occurs in the ordinary Hubbard model, while the entanglement spectrum for  $t_+$ -bonds still shows double

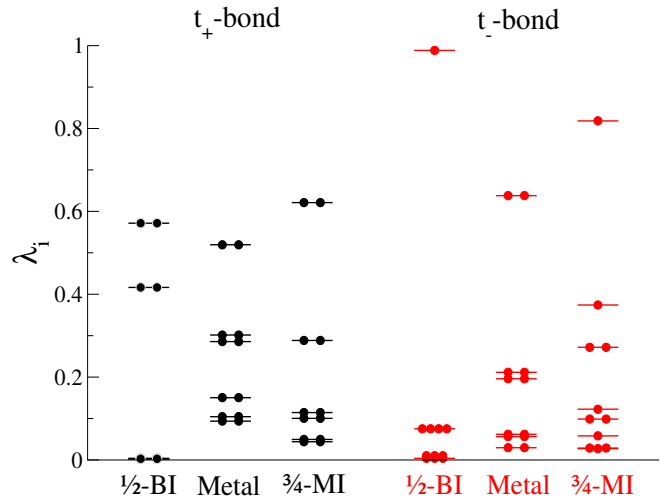


FIG. 4: Typical half-chain entanglement spectrum for  $t_+$ - and  $t_-$ -bonds at different phases of the dimerized Fermi-Hubbard model. In the metallic phase, the entanglement spectrum exhibits double degeneracy. This double degeneracy is lifted in the insulating phase for  $t_-$ -bonds, while  $t_+$ -bonds retain their double degeneracy, reflecting the spin-1/2 isospin state at 3/4-filling and the spin-singlet state at 1/2-filling.

degeneracy.

(2) At 3/4-filling, two sites connected by a  $t_+$ -bond can be viewed as a spin-1/2 isospin state, i.e.,  $\frac{1}{\sqrt{2}}(|\uparrow\downarrow, \uparrow\rangle + |\uparrow, \uparrow\downarrow\rangle)$  or  $\frac{1}{\sqrt{2}}(|\uparrow\downarrow, \downarrow\rangle + |\downarrow, \uparrow\downarrow\rangle)$ , which yields double degeneracy in the entanglement spectrum for  $t_+$ -bonds even in the insulating phase. These isospins then form an antiferromagnetic Mott insulating state through couplings mediated by  $t_-$ -bonds. This is very similar to what occurs in the half-filled Mott insulator in the ordinary Hubbard model, where the entanglement spectrum has a similar structure with a vanishing spin gap.

(3) For  $t_-$ -bonds at 1/2-filling,  $\lambda_1$ , the largest among the  $\lambda$ 's, is close to 1, implying that the system is nearly represented by a product state of two states: one on the left side and the other on the right side of a  $t_-$ -bond, with no diverging correlation length. As a result, the gap between  $\lambda_2$ , the second largest, and  $\lambda_1$  is quite large. Additionally, we observe almost quadruple degeneracy at the level of  $\lambda_2$ . This strongly suggests that the charge gap is indeed a band gap, such that the first excited states arise from single electron or single hole excitations with either spin up or spin down, leading to quadruple degeneracy. We also expect that the singlet state provides the double degeneracy in the entanglement spectrum for  $t_+$ -bonds. All these features, which are quite different from those observed in a Mott insulating phase at 3/4-filling, indicate that at 1/2-filling, we have a band insulating phase.

Above, we discuss that the insulating state at 3/4-filling will be a Mott insulator in which the spin-1/2 isospins are weakly coupled through  $t_-$ -bonds. Therefore, we expect the half-chain entanglement spectrum to exhibit the scaling behavior theoretically predicted by the

conformal field theory<sup>9,10</sup>.

Indeed, Figure 5 shows this scaling behavior for  $t_-$ -bonds in the Mott insulating phase at 3/4-filling. However, we do not observe this scaling behavior for  $t_+$ -bonds (i.e., data for different  $\chi$  do not collapse onto a single curve). This scaling behavior is also not observed at 1/2-filling (not shown in the figure). In the figure,  $n(w)$  represents the mean number of eigenvalues of the reduced density matrix (i.e.,  $w_\alpha \equiv \lambda_\alpha^2$ ) that are larger than a given  $w$  for different  $\chi$ , for  $t_-$ -bond (open symbols) and for  $t_+$ -bond (closed symbols) at 3/4-filling. The dotted line represents the theoretical prediction given by  $2I_0(\xi_w) - 1$  for one-dimensional critical systems with global degeneracy  $g = 2$ , where  $I_0(\xi_w)$  is the modified Bessel function of the first kind,  $\xi_w \equiv 2\sqrt{b \ln(w_1/w)}$ , and  $b \equiv \ln(w_1)$ .

The scaling properties of the entanglement spectrum exhibit the following two features: First, the entanglement spectrum for  $t_-$ -bond at 3/4-filling shows a universal distribution, similar to that observed in the spin-1/2 antiferromagnetic Mott insulator in the ordinary Hubbard model at half-filling. This indicates that it is a Mott insulator at 3/4-filling, in contrast to the 1/2-filled band insulator which does not exhibit the universal scaling properties. Second, the universal behavior at 3/4-filling shows the global degeneracy  $g = 2$ . Although a universal distribution with global degeneracy is theoretically predicted, no clear examples have been proposed. To our knowledge, this is the first non-trivial example to explicitly show the global degeneracy  $g = 2$  in the universal scaling behavior of the entanglement spectrum, where spin-half isospins form an antiferromagnetic Mott insu-

## IV. SUMMARY

We study the entanglement properties of the one-dimensional dimerized Fermi-Hubbard model through MPS representations. A phase diagram is constructed by investigating the entanglement entropy, revealing two insulating phases at 1/2-filling and 3/4-filling, separated by an intervening metallic phase. These phases can be identified by their distinct structures in the entanglement spectrum: the metallic phase exhibits double degeneracy in the distribution of the eigenvalues of the reduced density matrix, while in the insulating phases the degeneracy is lifted due to the presence of a finite charge gap. The entanglement entropy of the insulating phases indicates the presence (or absence) of the edge states, whose amount is modified by interactions. Furthermore, the scaling behavior of the half-chain entanglement entropy reveals the different nature of the two insulating phases: the insulating phase at 3/4-filling is a Mott phase with a diverging correlation length, while that at 1/2-filling is a band insulating phase with a finite short correlation length. This distinction is confirmed by the universal distribution of the entanglement spectrum, which is observed only at 3/4-filling, exhibiting the global degeneracy  $g = 2$ . All these results demonstrate that entanglement properties are a powerful tool for characterizing the nature, including topological properties, of interacting quantum systems.

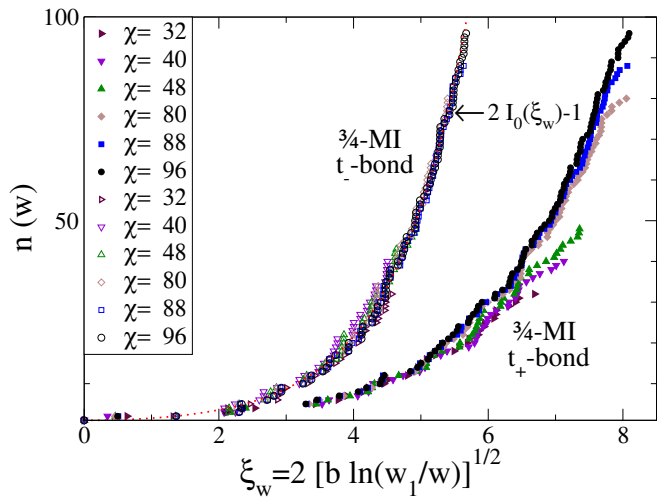


FIG. 5: The behavior of  $n(w)$ , the mean number of eigenvalues larger than a given  $w$ , for different  $\chi$  shows a universal scaling behavior for  $t_-$ -bonds in the 3/4-filled Mott insulating phase. No universal behavior is observed for  $t_+$ -bonds and in other phases (not shown in the figure). The dotted line represents the theoretical prediction given by  $2I_0(\xi_w) - 1$  with the global degeneracy  $g = 2$ .

## Acknowledgments

This work was supported by the Basic Science Research Program through the National Research Foundation of Korea funded by the Ministry of Education, Science and Technology (Grant No. NRF-2019R1F1A1062704 to MCC, Grant No. NRF-2021R1F1A1056081 to JWL, and Grant No. NRF-2021R1F1A1052347 to MHC).

- 
- <sup>1</sup> L. Amico, R. Fazio, A. Osterloh, and V. Vedral, Entanglement in many-body systems, *Rev. Mod. Phys.* **80**, 517 (2008).
- <sup>2</sup> R. Horodecki, P. Horodecki, M. Horodecki, and K. Horodecki, Quantum entanglement, *Rev. Mod. Phys.* **81**, 865 (2009).
- <sup>3</sup> P. Calabrese, J. Cardy, and B. Doyon, Entanglement entropy in extended quantum systems, *J. Phys. A: Math. Theor.* **42**, 500301 (2009).
- <sup>4</sup> N. Laflorencie, Quantum entanglement in condensed matter systems, *Phys. Rep.* **643**, 1 (2016).
- <sup>5</sup> P. Calabrese and J. Cardy, Entanglement entropy and conformal field theory, P. Calabrese and J. Cardy 2009 *J. Phys. A: Math. Theor.* **42**, 504005 (2009).
- <sup>6</sup> V. E. Korepin, Universality of Entropy Scaling in One Dimensional Gapless Models, *Phys. Rev. Lett.* **92**, 096402 (2004).
- <sup>7</sup> F. Pollmann, S. Mukerjee, A. M. Turner and J. E. Moore, Theory of Finite-Entanglement Scaling at One-Dimensional Quantum Critical Point, *Phys. Rev. Lett.* **102**, 255701 (2009).
- <sup>8</sup> L. Tagliacozzo, T. R. de Oliveira, S. Iblisdir, and J. I. Latorre, Scaling of entanglement support for matrix product states, *Phys. Rev. B* **78**, 024410 (2008).
- <sup>9</sup> P. Calabrese and A. Lefevre, Entanglement spectrum in one-dimensional systems, *Phys. Rev. A* **78**, 032329 (2008).
- <sup>10</sup> V. Alba, P. Calabrese, and E. Tonni, Entanglement spectrum degeneracy and the Cardy formula in 1+1 dimensional conformal field theories, *J. Phys. A* **51**, 024001 (2018).
- <sup>11</sup> M.-C. Cha, Quantum phase transitions in the matrix product states of the one-dimensional boson Hubbard model, *Phys. Rev. B* **106**, 235121 (2022).
- <sup>12</sup> A. Kitaev, and J. Preskill, Topological Entanglement Entropy, *Phys. Rev. Lett.* **96**, 110404 (2006).
- <sup>13</sup> M. Levin and X.-G. Wen, Detecting Topological Order in a Ground State Wave Function, *Phys. Rev. Lett.* **96**, 110405 (2006).
- <sup>14</sup> M. Z. Hasan and C. L. Kane, Colloquium: Topological insulators, *Rev. Mod. Phys.* **82**, 3045 (2010).
- <sup>15</sup> X. L. Qi and S. C. Zhang, Topological insulators and superconductors, *Rev. Mod. Phys.* **83**, 1057 (2011).
- <sup>16</sup> A. Bansil, H. Lin, and T. Das, Colloquium: Topological band theory, *Rev. Mod. Phys.* **88**, 021004 (2016).
- <sup>17</sup> X.-L. Qi, H. Katsura, and A. W. W. Ludwig, General Relationship between the Entanglement Spectrum and the Edge State Spectrum of Topological Quantum States, *Phys. Rev. Lett.* **108**, 196402 (2012).
- <sup>18</sup> G. De Chiara, L. Lepori, M. Lewenstein, and A. Sanpera, Entanglement Spectrum, Critical Exponents, and Order Parameters in Quantum Spin Chains, *Phys. Rev. Lett.* **109**, 237208 (2012).
- <sup>19</sup> S. Rachel, Interacting topological insulators: a review, *Rep. Prog. Phys.* **81**, 116501 (2018).
- <sup>20</sup> E. Tang and X.-G. Wen, Interacting one-dimensional fermionic symmetry-protected topological phases. *Phys. Rev. Lett.* **109**, 096403 (2012).
- <sup>21</sup> S. R. Manmana, A. M. Essin, R. M. Noack, and V. Gurarie, Topological invariants and interacting one-dimensional fermionic systems. *Phys. Rev. B* **86**, 205119 (2012).
- <sup>22</sup> H. M. Guo and S. Q. Shen, Topological phase in a one-dimensional interacting fermion system, *Phys. Rev. B* **84**, 195107 (2011).
- <sup>23</sup> N. Ara, R. Basu, E. Mathew, and I. Raychowdhury, Entanglement of edge modes in (very) strongly correlated topological insulators, *J. Phys.: Condens. Matter.* **36**, 295601 (2024).
- <sup>24</sup> D. Wang, S. Xu, Y. Wang, and C. Wu, Detecting edge degeneracy in interacting topological insulators through entanglement entropy, *Phys. Rev. B* **91**, 115118 (2015).
- <sup>25</sup> N. Wagner, L. Crippa, A. Amaricci, P. Hansmann, M. Klett, E. J. König, T. Schäfer, D. Di Sante, J. Cano, A. J. Millis, A. Georges, and G. Sangiovanni, Mott insulators with boundary zeros, *Nat. Commun.* **14**, 7531 (2023).
- <sup>26</sup> J. Zhao, P. Mai, B. Bradlyn, and P. Phillips, Failure of Topological Invariants in Strongly Correlated Matter *Phys. Rev. Lett.* **131** 106601 (2023).
- <sup>27</sup> W. P. Su, J. R. Schrieffer, and A. J. Heeger, Solitons in Polyacetylene, *Phys. Rev. Lett.* **42**, 1698 (1979).
- <sup>28</sup> J. K. Asbóth, L. Oroszlány, and A. Pályi, *A Short Course on Topological Insulators* (Springer International Publishing, 2016).
- <sup>29</sup> N.H Le, A. J. Fisher, N. J. Curson, and E. Ginossar, Topological phases of a dimerized Fermi-Hubbard model for semiconductor nano-lattices, *npj Quantum Inf.* **6**, 24 (2020).
- <sup>30</sup> D. Mikhail and S. Rachel, Su-Schrieffer-Heeger-Hubbard model at quarter filling: Effects of magnetic field and non-local interactions, *Phys. Rev. B* **110**, 205106 (2024).
- <sup>31</sup> S. Ryu and Y. Hatsugai, Entanglement entropy and the Berry phase in the solid state, *Phys. Rev. B* **73**, 245115 (2006).
- <sup>32</sup> J. Sirker, M. Maiti, N. P. Konstantinidis, and N. Sedlmayr, Boundary Fidelity and Entanglement in the symmetry protected topological phase of the SSH model, *J. Stat. Mech.* (2014) P10032.
- <sup>33</sup> J. Bisht, S. Jalal, and B. Kumar, Transmigration of edge states with interaction in Su-Schrieffer-Heeger chain, *Phys. Rev. B* **110**, 245110 (2024).
- <sup>34</sup> X. Zhou, S. Jia, and J.-S. Pan, Interaction-induced phase transitions at topological quantum criticality of an extended Su-Schrieffer-Heeger model, *Phys. Rev. B* **111**, 195117 (2025).
- <sup>35</sup> P.-J. Chang, J. Pi, M. Zheng, Y.-T. Lei, X. Pan, D. Ruan, and G.-L. Long, Topological phases of extended Su-Schrieffer-Heeger-Hubbard model *Sci. Rep.* **15**, 18023 (2025).
- <sup>36</sup> B.-T. Ye, L.-Z. Mu, and H. Fan, Entanglement spectrum of Su-Schrieffer-Heeger-Hubbard model, *Phys. Rev. B* **94**, 165167 (2016).
- <sup>37</sup> G. Vidal, Efficient Classical Simulation of Slightly Entangled Quantum Computations, *Phys. Rev. Lett.* **93**, 040502 (2004).
- <sup>38</sup> G. Vidal, Classical Simulation of Infinite-Size Quantum Lattice Systems in One Spatial Dimension, *Phys. Rev. Lett.* **98**, 070201 (2007).
- <sup>39</sup> M.-C. Cha, Finite-entanglement properties in the matrix product states of the one-dimensional Hubbard model, *Phys. Rev. B* **98**, 235161 (2018).
- <sup>40</sup> F. H. L. Essler, H. Frahm, F. Göhman, A. Klümper, V. E. Korepin, *The One-Dimensional Hubbard Model* (Cambridge University Press, Cambridge, 2005).